ARTICLE
Journal of Cellular Biochemistry 115:794–803 (2014)

Journal of Cellular Biochemistry

A Nanoscaffold Impregnated With Human Wharton's Jelly Stem Cells or Its Secretions Improves Healing of Wounds

Kimberley Tam,[1] Suganya Cheyyatraviendran,[1] Jayarama Venugopal,[2] Arijit Biswas,[1] Mahesh Choolani,[1] Seeram Ramakrishna,[2] Ariff Bongso,[1]* and Chui-Yee Fong[1]*

[1]*Department of Obstetrics and Gynaecology, Yong Yoo Lin School of Medicine, National University Health System, National University of Singapore, Kent Ridge, Singapore 119228, Singapore*

[2]*Department of Mechanical Engineering, Centre for Nanofibers and Nanotechnology, School of Engineering, National University of Singapore, Singapore 117576, Singapore*

ABSTRACT

Wound healing is a major problem in diabetic patients and current methods of treatment have met with limited success. Since skin cell renewal is under the control of mesenchymal stem cells (MSCs) treatment of wounds has been attempted with the application of exogenous bone marrow MSCs (hBMMSCs). However, hBMMSCs have the limitations of painful harvest, low cell numbers and short-lived stemness properties unlike MSCs from the Wharton's jelly of human umbilical cords (hWJSCs). Since nanoscaffolds provide three dimensional architectural patterns that mimic in vivo stem cell niches and aloe vera has antibacterial properties we evaluated the use of an aloe vera-polycaprolactone (AV/PCL) nanoscaffold impregnated with green fluorescent protein (GFP)-labeled hWJSCs (GFP-hWJSCs + AV/PCL) or its conditioned medium (hWJSC-CM + AV/PCL) for healing of excisional and diabetic wounds. In skin fibroblast scratch-wound assays exposed to GFP-hWJSCs + AV/PCL or hWJSC-CM + AV/PCL, fibroblasts migrated significantly faster from edges of scratches into vacant areas together with increased secretion of collagen I and III, elastin, fibronectin, superoxide dismutase, and metalloproteinase-1 (MMP-1) compared to controls. After one application of GFP-hWJSCs + AV/PCL or hWJSC-CM + AV/PCL excisional and diabetic wounds in mice showed rapid wound closure, reepithelialization, and increased numbers of sebaceous glands and hair follicles compared to controls. The same wounds exposed to GFP-hWJSCs + AV/PCL or hWJSC-CM + AV/PCL also showed positive keratinocyte markers (cytokeratin, involucrin, filaggrin) and increased expression of ICAM-1, TIMP-1, and VEGF-A compared to controls. AV/PCL nanoscaffolds in combination with hWJSCs appear to have synergistic benefits for wound healing. J. Cell. Biochem. 115: 794–803, 2014.

KEY WORDS: ALOE VERA-POLYCAPROLACTONE NANOSCAFFOLD; CONDITIONED MEDIUM; EXCISIONAL AND DIABETIC WOUNDS; HUMAN WHARTON'S JELLY STEM CELLS; WOUND HEALING

The process of wound healing requires an orchestrated integration of complex biological and molecular events, which include inflammation, proliferation, and remodeling [Shaw and Martin, 2009; Maxson et al., 2012]. Post-operative wounds and chronic non-healing wounds such as diabetic ulcers, bedsores, burns, venous, and arterial ulcers are major problems which are accentuated by ischemia to the affected areas, patient mobility, advanced age and disease [Brower et al., 2011; White-Chu et al., 2011; Shilo et al., 2013]. Such wounds if not treated effectively eventually end up in amputations or disfiguring scars termed keloids. Chemicals, dressings, and skin grafts used to date for their treatment have met with limited success.

Cells in the skin are renewed constantly and are under the control of mesenchymal stem cells (MSCs) residing in the epidermis, the hair bulb, the melanocyte layer and the dermis [Badiavas and Falanga, 2003]. The advantages of exogenous application of human bone marrow mesenchymal stem cells (hBMMSCs) on wound healing have been reported in several animal models and in the human [Maxson et al., 2012]. hBMMSCs improve wound healing by modulating the inflammatory environment, promoting angiogenesis, and

Conflict of interest: none.

Grant sponsor: National Research Foundation (NRF); Grant number: R-174-000-139-281; Grant sponsor: Academic Research Fund, National University of Singapore (AcRF-NUS); Grant number: R-174-000-122-112.

*Correspondence to: Ariff Bongso and Chui-Yee Fong, Department of Obstetrics and Gynaecology, Yong Loo Lin School of Medicine, National University Health System, National University of Singapore, Kent Ridge, Singapore 119228, Singapore. E-mail: obgbongs@nus.edu.sg, obgfong@nus.edu.sg

Manuscript Received: 8 November 2013; Manuscript Accepted: 18 November 2013

Accepted manuscript online in Wiley Online Library (wileyonlinelibrary.com): 22 November 2013

DOI 10.1002/jcb.24723 • © 2013 Wiley Periodicals, Inc.

vascularization, encouraging the migration of keratinocytes and inhibiting apoptosis of wound healing cells [Jackson et al., 2012]. However, hBMMSCs have their limitations in that they involve painful harvest with potential risk of infection and morbidity to the patient, their numbers in the bone marrow are low and they retain their stemness properties in vitro only for a few passages. Recently, human umbilical cord Wharton's jelly stem cells (hWJSCs) were shown to have better clinical utility because of their unique advantages over hBMMSCs such as their availability in large numbers, prolonged stemness properties in vitro, their non-controversial nature and painless harvest [Bongso and Fong, 2013].

Cells respond best to their in vivo environment at nanoscale (nm) levels and the natural proteins of the extracellular matrix (ECM) are usually in the range of 50–500 nm which interestingly is similar to the diameter of nanofibers. Thus, scaffolds made up of nanofibers have the advantages of (i) three dimensional (3D) architectural nanoscale patterns that mimic the in vivo stem cell niche providing cues for stem cells to attach and differentiate into host cells, (ii) a large surface-to-volume ratio and (iii) good porosity to allow penetration of nutrients and growth factors from stem cells for tissue repair. Furthermore, nanoscaffolds could be designed to biodegrade at required times allowing the stem cells to complete healing until wound closure. Polycaprolactone (PCL) has been the conventional chemical of choice to prepare such nanoscaffolds [Ma et al., 2011] while aloe vera which is a well-known antibacterial agent contains acetylated mannans that have been shown to promote wound healing by reducing inflammation, providing tensile strength and preventing infection [Vazquez et al., 1996; Hamman, 2008; Mendonca et al., 2009; Takzare et al., 2009]. In a recent report we showed that hWJSCs or its extracts (hWJSC conditioned medium, hWJSC-CM) alone without a scaffold enhanced healing of excisional and diabetic wounds. Since the benefits of including a scaffold to provide stem cells their niches for attachment and sustained release of important bioactive molecules for improved wound healing have not been evaluated, we explored the use of a wound dressing patch made up of an aloe vera-PCL (AV/PCL) nanoscaffold impregnated with hWJSCs or its conditioned medium (hWJSC-CM) for enhanced healing of excisional and diabetic wounds in in vitro and in vivo.

MATERIALS AND METHODS

CELL CULTURE, CELL LABELLING AND PREPARATION OF CONDITIONED MEDIUM

Ethical approval for the use of discarded human umbilical cords for this study was given by the Institutional Domain Specific Review Board (DSRB), Singapore. hWJSCs were derived and characterized according to our published protocols [Fong et al., 2007, 2010]. Human foreskin fibroblasts (CCD-112sk) (abbreviated as CCD) were obtained from the American Type Culture Collection (ATCC, MD) to act as controls and ethical approval for their use was given by the National University of Singapore Institutional Review Board (NUS-IRB). hWJSCs and CCDs were transduced with a lentiviral vector for green fluorescence protein (GFP-hWJSCs, GFP-CCDs) for cell identification and tracking purposes [Fong et al., 2013]. GFP-hWJSCs and GFP-CCDs (passages 3–4) were grown in a serum-free knock-out basal medium supplemented with serum replacement substitute (KOSR medium) to avoid contamination by serum proteins. After 72 h, the conditioned media (hWJSC-CM, CCD-CM) were separated, sterilized with a 0.22 μm filter (Millipore, Billerica, MA) and diluted with KOSR medium to make 50% conditioned medium.

FABRICATION AND CHARACTERIZATION OF AV/PCL NANOSCAFFOLDS

Polycaprolactone (PCL) (MW: 80,000) (Sigma–Aldrich, St. Louis, MO) and aloe vera freeze-dried powder (Zhang Peng International, Singapore) were dissolved (15% v/w) (10% PCL:5% aloe vera) in chloroform:methanol (3:1) (Sigma–Aldrich) by stirring for 24 h. To prepare topographically randomized nanoscaffolds, the aloe vera-PCL mixture was electrospun after feeding into a 3 ml syringe attached to a 18G blunt stainless steel needle and using a syringe pump at a flow rate of 3.0 ml/h with an applied voltage of 25 kV (Nanon, Mecc, Fukuoka, Japan). The nanofibers were collected and spread at 23°C and 45% humidity from a rotating drum on to 15 mm cover slips. The mean ± SEM diameter of the nanofibers was calculated using scanning electron microscopy (SEM). Nanoscaffolds were vacuum-dried and sterilized before use.

PREPARATION OF WOUND DRESSING PATCHES

The preparation of the wound dressing patch is described schematically in Figure 1. Two types of patches were prepared. (1) Sterile nanoscaffolds seeded with GFP-hWJSCs or GFP-CCDs (5×10^5 cells) followed by incubation for 72 h at 37°C in a 5% CO_2 in air atmosphere. These were examined under confocal microscopy (Olympus FV 1000) to ensure that the cells had attached and migrated into the nanoscaffolds (Fig. 1). (2) Separately, nanoscaffolds were impregnated with hWJSC-CM or CCD-CM over 72 h (Fig. 1).

IN VITRO STUDIES

Scratch-wound assays. The conventional skin fibroblast scratch-wound assay of Cory [2011] for wound healing was adopted. Firstly, CCDs were cultured on 0.1% gelatin-coated 60 mm Petri dishes (Nalgene NUNC International, Rochester, NY) in KOSR medium at 37°C in a 5% CO_2 in air atmosphere for 24 h to produce confluent monolayers. Linear scratches (0.5 mm width) to mimic wounds were made vertically from top to bottom along the midline of confluent CCD monolayers using a sterile pipette. The spent KOSR culture medium from the Petri dish was then removed together with the detached CCD cells. Nanoscaffolds that were pre-soaked in hWJSC-CM, or CCD-CM, or unconditioned KOSR medium were then placed over the respective wounds. Each Petri dish was then filled with 2 ml of its respective culture medium as follows: (i) hWJSC-CM + AV/PCL (treatment arm); (ii) CCD-CM + AV/PCL (control) and (iii) Unconditioned KOSR medium (UCM) + AV/PCL (control). Treatment and control dishes were then incubated at 37°C in a 5% CO_2 in air atmosphere for 72 h. Three replicates were carried out for each assay. CCD migration from the edges of the wounds into the vacant areas was monitored regularly and digitized images of at least five random fields within the wounds were taken every 24 h using inverted phase contrast optics for 72 h or until full closure of the wounds. Markings on the Petri dishes were used as reference points to monitor the same fields every 24 h. The mean ± SEM percentage extent of closure of the wounds at 24, 48, and 72 h were calculated from the digitized images

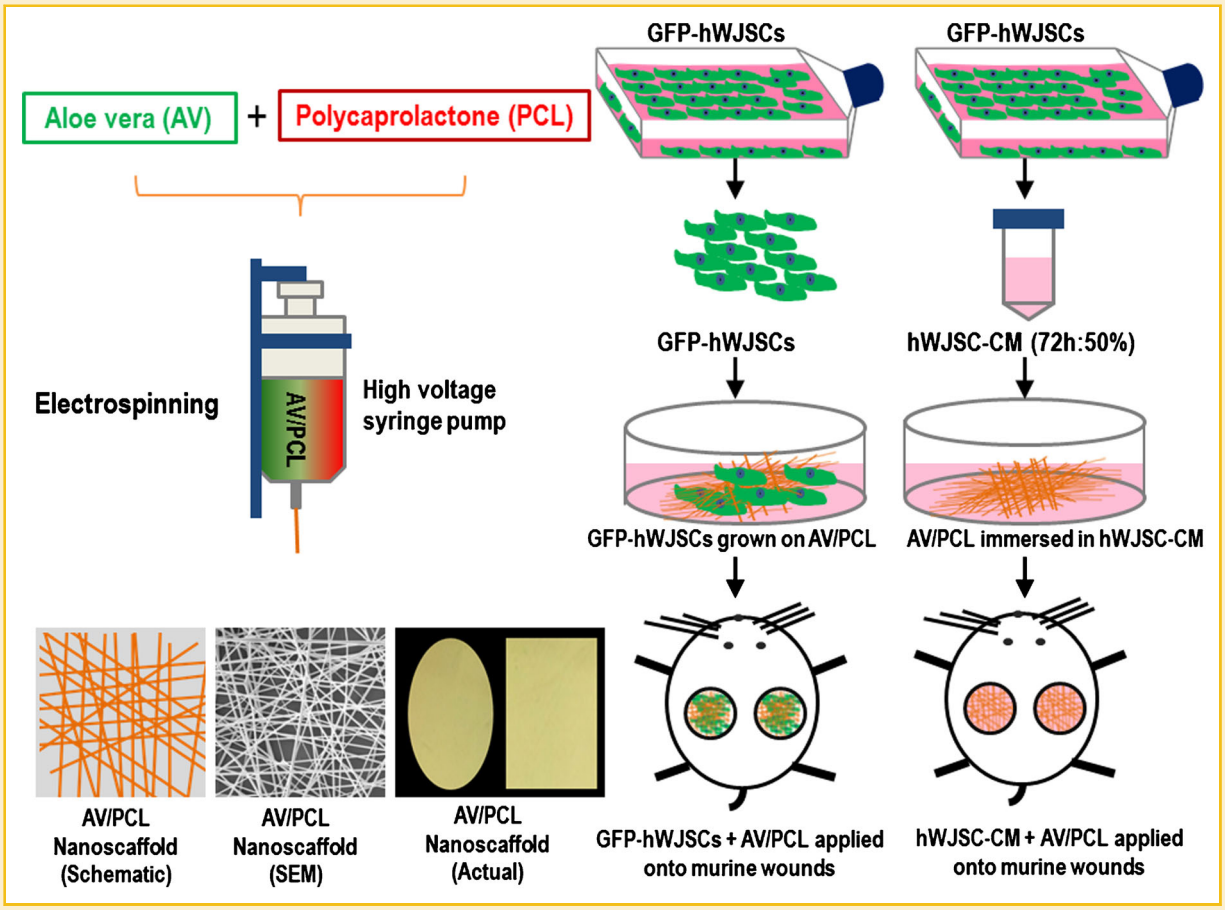

Fig. 1. Schematic diagram showing preparation of wound dressing patch. AV/PCL nanoscaffolds were prepared by electrospinning and then impregnated with either GFP-hWJSCs or hWJSC-CM.

using an image software program [Walter et al., 2010]. The number of viable CCDs in the scratch wounds was measured using the MTT assay to find out whether the respective treatments had stimulated CCD proliferation and survival, in addition to migration. The MTT assay was carried out using a MTT reagent kit [3-(4, 5-dimethylthiazolyl-2)-2, 5-diphenyltetrazolium bromide] (Sigma) according to the manufacturer's instructions. Absorbance at 570 nm was spectrophotometrically measured using a microplate ELISA reader (μQuant-BioTek, Winooski, VT) with a reference wavelength of 630 nm.

Collagen, elastin, superoxide dismutase (SOD) and qRT-PCR analysis. Total collagen, elastin, and SOD levels in treatment and control dishes were evaluated using Sircol™, Fastin™ (Biocolor, Carrickfergus, UK) and SOD (Sigma) kits respectively according to the manufacturer's instructions. The CCDs of treatment and control dishes were also subjected to conventional qRT-PCR using SYBR green and the ABI PRISM 7500 Fast Real-Time PCR System (Applied Biosystems, Foster City, CA) and relative quantification was performed using the comparative CT ($2^{-\Delta\Delta C_t}$) method. Primer sequences were taken from earlier published studies and are shown in Table I.

IN VIVO STUDIES

Excisional and diabetic wound mouse models. Approval for all animal procedures was given by the Institutional Animal Care and Use Committee (IACUC) of the National University of Singapore.

For the excisional wound study, female severely combined immunodeficient (SCID) mice (5–6 weeks) (Animal Resources Centre,

TABLE I. Primer Sequences Used for Quantitative Reverse Transcription-PCR Gene Expression Analysis

Gene	Primer sequence
Collagen III	F: 5′-CTGAAATTCTGCCATCCTGAAC-3′ R: 5′-GGATTGCCGTAGCTAAACTGAA-3′
Fibronectin	F: 5′-AAGATTGGAGAGAAGTGGGACC-3′ R: 5′-GAGCAAATGGCACCGAGATA-3′
MMP-1	F: 5′-TTGAGAAAGCCTTCCAACTCTG-3′ R:5′-CCGCAACACGATGTAAGTTGTA-3′
GAPDH	F: 5′-GCACCGTCAAGGCTGAGAAC-3′ R: 5′-GGATCTCGCTCCTGGAAGATG-3′

MMP, matrix metalloproteinase; GAPDH, glyceraldehyde-3-phosphate dehydrogenase.

Western Australia) were shaved after isofluorane anesthesia and two circular punch biopsy (Accusharp Punch, Pune, India) full-thickness wounds (8 mm diameter) were created on the left and right dorsal regions. Fifty-four mice (108 wounds) were divided into six groups [9 mice (18 wounds) per group] and the wounds in each group treated as follows [Gp 1 (treatment): GFP-hWJSCs (1×10^6 cells) + AV/PCL; Gp 2 (treatment): hWJSC-CM (100 μl) + AV/PCL; Gp 3 (control): GFP-CCDs (1×10^6 cells) + AV/PCL; Gp 4 (control): CCD-CM (100 μl) + AV/PCL; Gp 5 (control): PBS (100 μl) + AV/PCL and Gp 6 (control): untreated (No AV/PCL)]. The wounds of all six groups were covered with Tegaderm (3M) and the edges sealed with Dermabond™ (Ethicon, Johnson and Johnson, NJ) to prevent the animals from removing the Tegaderm. The animals were individually housed under a 12:12 h light-dark cycle under SPF conditions. Three mice from each group were randomly culled on days 3, 7, and 14 for excisional wound healing analysis.

For the diabetic wound study, similar full-thickness circular (6 mm diameter) wounds were created on the shaved dorsal regions (left and right) of diabetic mice (Strain BKS.Cg-Dock7^m+/+*Lepr*^{db}/J; Stock No: 000642 resembling Type IIDM) (The Jackson Laboratory, Bar Harbor, Maine). A smaller-sized wound punch was chosen to mimic other published murine diabetic wound studies [Sullivan et al., 2004; Wu et al., 2007]. Glucose levels were measured before and after the experiment to confirm that the mice were diabetic. A total of 36 mice (72 wounds) were divided into three groups [12 mice per group (24 wounds)] and the wounds in each group treated as follows: [Gp 1 (treatment): GFP-hWJSCs (1×10^6 cells) + AV/PCL; Gp 2 (treatment): hWJSC-CM (100 μl) + AV/PCL; Gp 3 (control): UCM (100 μl) + AV/PCL]. Four mice from each group were randomly sacrificed on days 7, 14, and 28 for diabetic wound healing analysis.

Digitized photographs were taken on days 0, 7, and 14 for excisional and on days 0, 14, and 28 for diabetic wounds. Excisional and diabetic wound healing rates until wound closure were calculated from the digitized images using a NIH recommended formula and image software (original wound area − new wound area)/original wound area × 100) [Chen et al., 2009] by two independent observers blinded to treatments.

At specific time points, biopsies from excisional and diabetic wounds were collected and frozen for fluorescent microscopy for the presence and survival of green-labelled hWJSCs or CCDs and for immunohistochemistry of human keratinocyte markers (filaggrin, involucrin, and cytokeratin) using mouse monoclonal anti-human filaggrin (Abcam, Cambridge, UK), anti-human involucrin (Genway, San Diego, CA) and anti-human cytokeratin (clone AE1/AE3) (Dako, Carpinteria, CA). Biopsies were also fixed in 10% buffered formalin for histology and snap-frozen in liquid nitrogen for genomic and molecular analysis.

Quantitative real-time PCR of wound biopsies. The mRNA expression of ICAM-1, TIMP-1 and VEGF-A in excisional and diabetic wound biopsies was examined using the TaqMan qRT-PCR protocol. Briefly, wound biopsies were homogenized using the TissueLyser LT (Qiagen, Valencia, CA) machine. Total RNA was then extracted using the EZ1 RNA Universal tissues kit (Qiagen) and reverse transcribed using a high capacity cDNA Reverse Transcription Kit (Applied Biosystems, Carlsbad, CA). TaqMan Fast Advance Mastermix (Applied Biosystems) was used for quantification of cytokine release and VEGF expression (TIMP-1: Mm00441818_m1, ICAM-1: Mm00516023_m1 and VEGF-A: Mm01281449_m1), respectively. All TaqMan Gene Expression Assays were performed against the endogenous reference gene GAPDH: Mm99999915_g1.

Statistical analysis. The results of in vitro studies were expressed as mean ± SEM from three different replicates for individual assays and the differences between treatments and controls were compared using Students *t*-test. For in vivo analyses, the mean ± SEM percentages of wound closure were analyzed by ANOVA and post-hoc test with Tukey's Honestly Significant Difference (HSD). A P value of <0.05 was regarded as statistically significant. Statistical significance was determined using SPSS software, version 13.0 (SPSS, Chicago, IL).

RESULTS

INTERACTION OF AV/PCL AND hWJSCs

Scanning electron micrographs showed that AV/PCL nanofibers electrospun on a rotating drum in our laboratories yielded a randomized mesh-like topography with mean ± SEM fiber diameters of 448 ± 65 nm, thickness of 0.5 mm and 90% porosity (Fig. 2a and b). There were adequate niches for the hWJSCs to attach, migrate and grow (Fig. 2c). Compilation of z-stack images via confocal laser microscopic imaging showed that after 48–72 h in culture GFP-hWJSCs were able to migrate into a depth of 51.3 μm into the nanoscaffold (Fig. 2d and e). The nanoscaffolds could be fabricated into different shapes for different sized wounds (Fig. 2f).

SCRATCH-WOUND ASSAY

CCDs started to migrate from the edges of the wounds into the vacant areas as early as 6–8 h in treatment and control dishes (Fig. 3A). Cell migration was more pronounced and the wounds were completely covered by days 2–3 (D2–D3) in the hWJSC-CM + AV/PCL treatment arm compared to controls (Fig. 3A). Wound closure rates (mean ± SEM %) were significantly greater in the hWJSC-CM + AV/PCL treatment arm compared to controls ($P < 0.05$; Fig. 3B). The actual mean ± SEM CCD numbers that migrated into the scratch areas for hWJSC-CM + AV/PCL (treatment), CCD-CM + AV/PCL (control) and UCM + AV/PCL (control) as determined by two independent observers were (24 h): 22 ± 02, 19 ± 02, 17 ± 02; (48 h): 58 ± 05, 32 ± 02, 33 ± 03; (72 h): 322 ± 04, 255 ± 04, and 158 ± 05 respectively. The viability of CCDs (MTT assay) from the hWJSC-CM + AV/PCL treatment arm was significantly greater than the controls (Fig. 3C).

The secreted total collagen, elastin and SOD concentration levels in scratch-wound assays were significantly greater in the treatment group (hWJSC-CM + AV/PCL) compared to the controls ($P < 0.05$; Fig. 3D–F).

CCDs of scratch-wound assays in the treatment arm (hWJSC-CM + AV/PCL) showed significantly greater expression of collagen III and fibronectin compared to controls ($P < 0.05$) with 90- and 31-fold increases, respectively (Fig. 3G and H). Although MMP-1 expression was increased for the hWJSC-CM + AV/PCL treatment arm, the increase was not significantly different from controls (Fig. 3I).

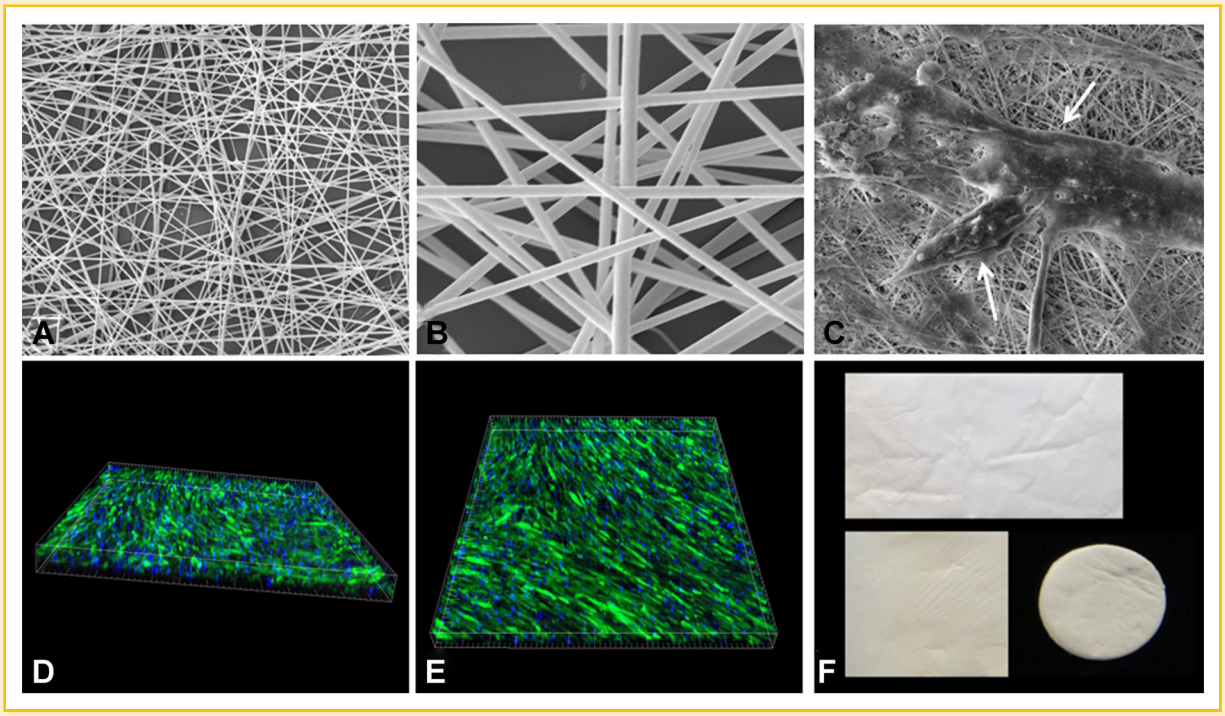

Fig. 2. (A and B) Low and high magnification scanning electron micrographs of AV/PCL randomly aligned nanofibers showing pores and niches (2,500×; 15,000×). (C) Scanning electron micrograph showing hWJSCs attached and growing on nanofibers (2,500×). (D and E) Confocal fluorescent images of side and surface views of AV/PCL nanoscaffolds impregnated with GFP-hWJSCs after 72 h. Note GFP-hWJSCs growing into nanoscaffold. (F) Final actual wound dressing patches of different shapes.

WOUND HEALING IN VIVO

A comparison of macroscopic digitized images of excisional wounds between treatment and control groups are shown in Figure 4A. Close monitoring of wound closure by two independent observers showed rapid wound closure by day 14 in the hWJSCs + AV/PCL and hWJSC-CM + AV/PCL arms compared to controls (Fig. 4A). Mean ± SEM percentage wound closure rates as determined by the wound healing formula on digitized images [Chen et al., 2009] showed that the hWJSCs + AV/PCL and hWJSC-CM + AV/PCL treatment arms exhibited faster wound closure compared to controls on day 7 with the closure rates for the hWJSCs + AV/PCL arm being significantly different from controls ($P < 0.05$). On day 14, the rate of wound closure was significantly greater in the hWJSCs + AV/PCL treatment arm compared to all other arms (Fig. 4B). On day 3, histological examination of wound biopsies in treatment groups demonstrated increased granulation and reepithelialization and appearance of a few sebaceous glands and hair follicles. On the other hand, the wound biopsies of controls showed disrupted epithelium, infiltration of leukocytes, lymphocytes, and fibroblasts in the dermis and the wound surfaces were covered with blood, fibrin and exudates (Fig. 4C). On days 7 and 14, the epidermis of wounds in the treatment arms (GFP-hWJSCs + AV/PCL and hWJSC-CM + AV/PCL) showed the formation of stratified squamous epithelium, increased numbers of sebaceous glands and hair follicles and greater cellularity and vasculature compared to controls (Fig. 4C).

A comparison of macroscopic digitized images and wound closure rates of diabetic wounds between treatment and control groups are shown in Figure 5A and B. The GFP-hWJSCs + AV/PCL and hWJSC-CM + AV/PCL treated mice showed complete wound closure of diabetic wounds compared to UCM + AV/PCL (control) by day 28 (Fig. 5A). On day 7, the mean ± SEM percentage rate of wound closure of the GFP-hWJSCs + AV/PCL treatment arm was significantly greater than the controls and on day 14 the wound closure rates of the hWJSC-CM + AV/PCL treatment group was significantly greater than the controls ($P < 0.05$; Fig. 5B). On day 7, histological examination of the diabetic wound biopsies showed reepithelialization, a few sebaceous glands and some hair follicles in the treatment groups compared to the controls. On days 14 and 28 the treatment groups (GFP-hWJSCs + AV/PCL and hWJSC-CM + AV/PCL) showed the formation of stratified squamous epithelium, increased cellularity and vasculature and increased sebaceous gland and hair follicle numbers compared to controls. On day 28 the diabetic wounds of controls not receiving any treatment had no stratified squamous epithelium, only a few sebaceous glands and hair follicles and as such did not display the typical normal skin phenotype (Fig. 5C). Immunofluorescence staining of cytokeratin, involucrin, and filaggrin which are markers of epidermal differentiation [Kawachi et al., 2011] are shown in Figure 5D. Positive staining for cytokeratin was present on days 14 and 28 in db/db mice (Fig. 5D, a, d: short arrows). Involucrin, a marker for epidermal late-stage differentiation was evident on day 14 (Fig. 5D, b: short arrow) and filaggrin, a marker for terminally differentiated granular layer keratinocytes was present on day 28 (Fig. 5D, f: short arrow).

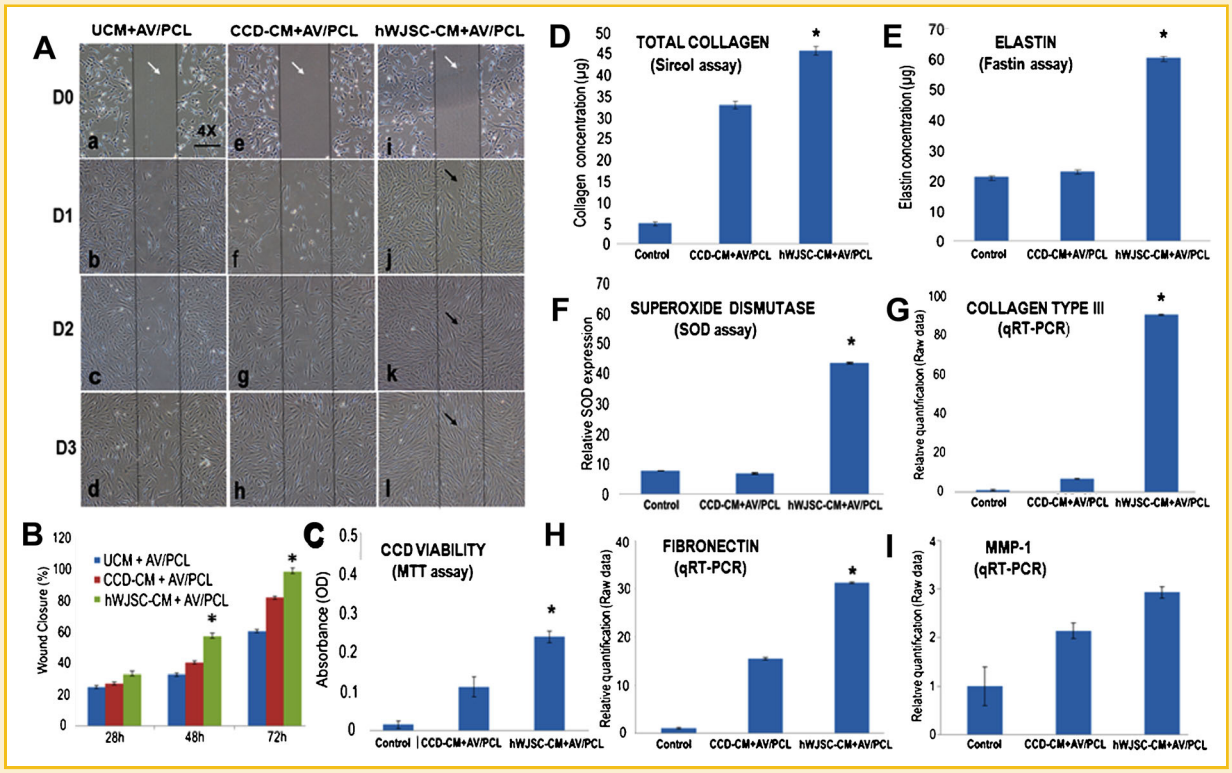

Fig. 3. (A) Scratch-wound assays of CCD fibroblasts (72 h; D0–D3) exposed to hWJSC-CM + AV/PCL (treatment), CCD-CM + AV/PCL (control) and UCM + AV/PCL (control). (a–i) Note vacant linear scratches (wounds) with no cells (white arrows) in treatment and controls assays on D0. (b–j) Note CCDs migrating from edges of wounds into vacant areas on D1 with greatest migration in hWJSC-CM + AV/PCL treatment group (black arrow). (c–k and d–l) Note faster migration of CCDs on D2 and D3 in hWJSC-CM + AV/PCL treatment group with wounds fully covered by D2 and D3 compared to controls. (B) Histogram showing that mean ± SEM wound closure percentages were significantly greater in the hWJSC-CM + AV/PCL treatment group compared to controls ($P < 0.05$). (C–F) Histogram showing that cell viability, total collagen, elastin and SOD concentrations in scratch-wound assays were significantly greater in the hWJSC-CM + AV/PCL treatment group compared to controls ($P < 0.05$). (G–I) Histogram showing that the qRT-PCR cDNA expression levels of collagen III and fibronectin in scratch-wound assays were significantly greater in the hWJSC-CM + AV/PCL treatment groups compared to controls ($P < 0.05$) while MMP-1 although greater were no significantly different from controls.

DIFFERENTIAL GENE EXPRESSION IN EXCISIONAL AND DIABETIC WOUNDS

ICAM-1 mRNA levels in excisional wounds in mice treated with GFP-hWJSCs + AV/PCL were significantly higher than controls on day 7 while TIMP-1 and VEGF-A expression for the hWJSC-CM + AV/PCL group was significantly higher than all other groups on day 14 ($P < 0.05$; Fig. 6A). For diabetic wounds, the TIMP-1 levels for both the treatment groups (GFP-hWJSCs + AV/PCL and hWJSC-CM + AV/PCL) were significantly higher on day 14 compared to other groups while VEGF-A expression however was significantly higher only for the GFP-hWJSCs + AV/PCL treatment group compared to other groups on day 14 ($P < 0.05$; Fig. 6B).

DISCUSSION

The main aim of engineered tissue regeneration is the construction of a biocompatible scaffold that when impregnated with viable cells and/or bioactive molecules can replace, regenerate, or repair damaged tissues [Tocco et al., 2012]. Bioengineered constructs for wound healing need to mimic the dermis by adhering to and integrating with the wound and in many instances this is unsuccessful. Artificial dermal analogues are costly making their application prohibitive [Tocco et al., 2012]. The use of nanofibrous scaffolds has drawn tremendous enthusiasm in skin tissue engineering because electrospinning technology serves as a simple platform to generate such matrices that can take the form and function of the ECM of skin. Nanoscaffolds mimic the fibrous architecture of the ECM and support cell adhesion, proliferation and differentiation. Furthermore, the large surface area and porosity of electrospun nanofibers allow good permeability for oxygen and water and the adsorption of liquids and protects the wound from bacterial penetration and dehydration. The surface topography of nanofibers and the grooves and ridges within them are known to be important contributors to cell attachment and these features have been shown to encourage MSCs to readily adhere to them [Ma et al., 2011]. Nanofibers are thus ideal material for wound dressings particularly for chronic wounds such as diabetic ulcers or burns [Tocco et al., 2012]. In a recent previous study we reported the effectiveness of hWJSCs or hWJSC-CM alone without the presence of an AV/PCL nanoscaffold in excisional and diabetic wound healing [Fong et al., 2013]. In the present study, we highlight the benefits of an AV/PCL nanoscaffold impregnated with hWJSCs or its conditioned

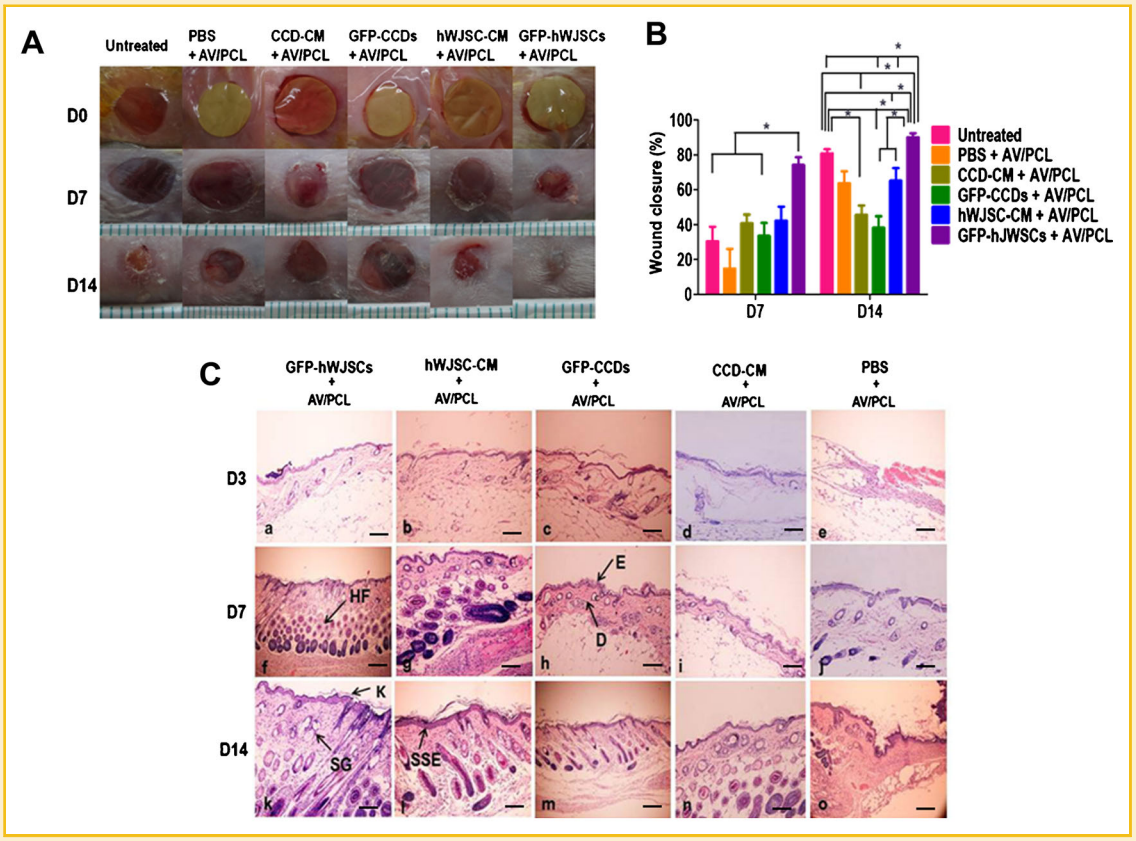

Fig. 4. (A) Digitized images of excisional wounds in SCID mice showed faster wound closure by day 7 in the GFP-hWJSCs + AV/PCL treatment arm compared to all other arms. (B) Mean ± SEM percentage wound closure rates in SCID mice were significantly faster in the GFP-hWJSCs + AV/PCL arm compared to controls on day 7 ($P < 0.05$). On day 14, wound closure rates were significantly greater in the GFP-hWJSCs + AV/PCL and hWJSC-CM + AV/PCL arms compared to controls ($P < 0.05$). (C) Representative hematoxylin and eosin histological sections of excisional wound biopsies taken on days 3, 7, and 14 (4–7 histological sections were examined for each group). (a–e) On day 3, wound biopsies in the GFP-hWJSCs + AV/PCL and hWJSC-CM + AV/PCL treatment groups showed increased granulation, reepithelialization and appearance of a few sebaceous glands and hair follicles while controls showed disrupted epithelium and wound surfaces covered with blood, fibrin and exudates (f–j and k–o). On days 7 and 14, the epidermis of wounds in the treatment arms (GFP-hWJSCs + AV/PCL and hWJSC-CM + AV/PCL) showed the formation of stratified squamous epithelium, increased numbers of sebaceous glands and hair follicles and greater cellularity and vasculature compared to controls. D, dermis; E, epidermis; HF, hair follicle; K, keratin; SG, sebaceous gland; SSE, stratified squamous epithelium. Scale bar = 100 μm.

medium as novel dry or wet wound dressings for surgical and diabetic wounds. Since cells perform best in the presence of three dimensional cues, the enhanced efficiency of wound healing in the two treatment groups (hWJSCs + AV/PCL and hWJSC-CM + AV/PCL) of the present study may be attributed to the synergistic effect of stem cells and nanoscaffold where the nanoscaffold provided the stem cell niches and porosity for the hWJSCs to attach, differentiate and allow its secretions to penetrate into the wound beds.

Aloe vera is rich in anthraquinones [Kuzuya et al., 2001] which are potent antibacterial agents. The antibacterial properties of aloe vera against *Bacillus subtilis, Escherichia coli*, and *Staphylococcus aureus* have been demonstrated [Ndhlala et al., 2009]. Its presence in the AV/PCL nanoscaffold provides a complementary benefit to wound healing thus explaining why none of the wounds were infected in this study in spite of the mice not being administered antibiotics. It has also been reported that aloe vera accelerates the tissue proliferation phase encouraging fibroplasia and collagen synthesis thus promoting better wound healing [Chithra et al., 1998].

Since both the hWJSCs and its conditioned medium showed significantly better wound healing over controls, cell-to-cell contact and non-cellular contact mechanisms (via the release of important molecules) may have facilitated the wound healing process. Human umbilical cord MSCs were shown to differentiate into keratinocytes when administered locally into the wound beds of mice [Luo et al., 2010; Fong et al., 2013]. The presence of GFP-hWJSCs or secreted bioactive molecules (from hWJSC-CM) within the wounds probably stimulate the recruitment of native skin MSCs and progenitor cells to the wound site to facilitate healing as suggested recently by Shin and Peterson [2013].

In preliminary studies we observed that specific miRNA clusters (miR-106a-363, miR-17-92, miR-106b-25, miR-302-367, and miR-21) were highly expressed in hWJSCs compared to hBMMSCs. The miR-106a-363 and miR-17-92 clusters are involved in cell proliferation and growth thus playing a role in the wound healing process. MiR-106b-25 upregulation leads to increased binding to collagen and the ECM while miR-302-367 is known to target TGFβ

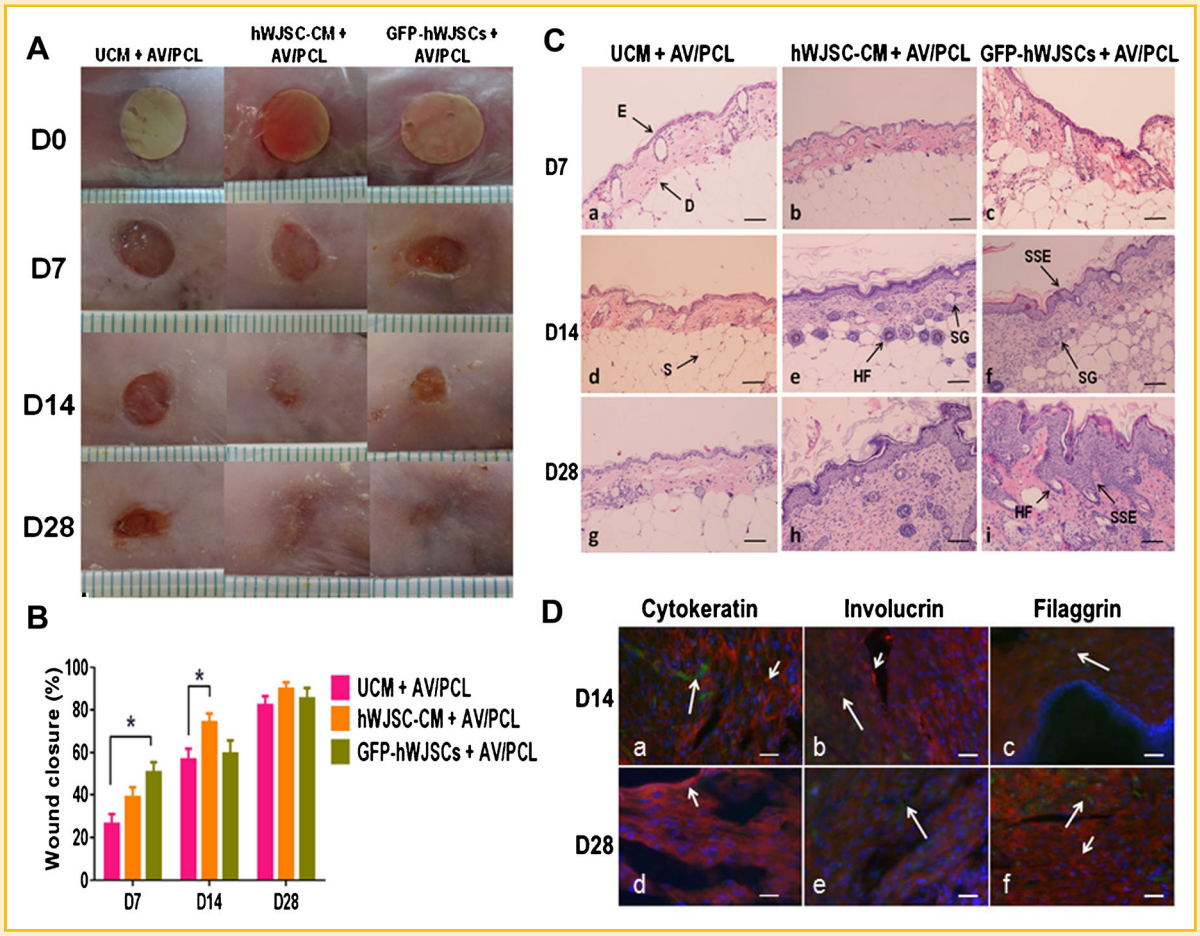

Fig. 5. (A) Digitized images of diabetic wounds in db/db mice showed complete wound closure in the GFP-hWJSCs + AV/PCL and hWJSC-CM + AV/PCL treatment arms compared to controls by day 28. (B) On day 7, the mean ± SEM percentage wound closure rates of the GFP-hWJSCs + AV/PCL treatment arm of diabetic wounds was significantly greater than the controls while on day 14 that of the hWJSC-CM + AV/PCL treatment group was significantly greater than the controls ($P < 0.05$). (C) On day 7, histological examination of diabetic wound biopsies showed reepithelialization, sebaceous glands and hair follicles in the GFP-hWJSCs + AV/PCL and hWJSC-CM + AV/PCL treatment groups compared to controls. On days 14 and 28 the same treatment groups showed the formation of stratified squamous epithelium, increased cellularity and vasculature and increased sebaceous gland and hair follicle numbers compared to controls. On day 28 the diabetic wounds of controls not receiving any treatment had no stratified squamous epithelium, only a few sebaceous glands and hair follicles and did not display the typical normal skin phenotype. D, dermis; E, epidermis; HF, hair follicle; SG, sebaceous gland; S, stroma; SSE, stratified squamous epithelium. Scale bar: 100 μm. (D: a, d) Positive staining for human cytokeratin was present on days 14 and 28 in diabetic wounds while human involucrin was evident on day 14 and human filaggrin was present on day 28. Long arrows: Viable GFP-hWJSCs in diabetic wound biopsies. Short arrows: Positive human keratinocyte markers (cytokeratin, involucrin, and filaggrin).

receptor 2 to encourage E-cadherin expression and promote mesenchymal-to-epithelial transition for improved reepithelialization [Liao et al., 2011]. Madhyastha et al. [2012] showed that miR-21 is upregulated on day 8 in the normal wound healing process and Ji et al. [2007] demonstrated that it exhibits proliferative and anti-apoptosis properties on vascular smooth muscle cells thus enhancing angiogenesis for better wound healing. The gene expression profiles of wound biopsies in the present study showed the upregulation of VEGF-A. Interestingly, our miRNA and proteomics pilot studies showed that the VEGF-induced miRNAs (miR-191, -155, -31, -17-5p, -18a and -20a) were significantly upregulated in hWJSCs compared to CCDs and hBMMSCs. It is also well-known that VEGF is an important player in the wound healing process [Bao et al., 2009].

ICAM-1 is central to the regulation of the inflammatory process during wound healing in the human and mouse and assists in cell adhesion of the ECM. Impaired wound healing is also associated with high levels of matrix metalloproteinases (MMPs) and low levels of the tissue inhibitors of MMPs (TIMPs) in chronic wound beds [Liu et al., 2009; Stevens and Page-McCaw, 2012]. It is interesting to note that in the present study the high levels of TIMP-1 in hWJSC-CM may have reversed the MMP/TIMP ratio thus facilitating wound healing and this is synergistic at a transcriptional level with the increases in gene expression of fibronectin, collagen I and III indicating that hWJSCs release proteins which affect ECM remodeling.

Fibroblasts in wounds modulate fibroblast-keratinocyte-endothelium interaction through the production of the ECM and cytokines [Jeon et al., 2010] and we have shown that hWJSCs release a variety

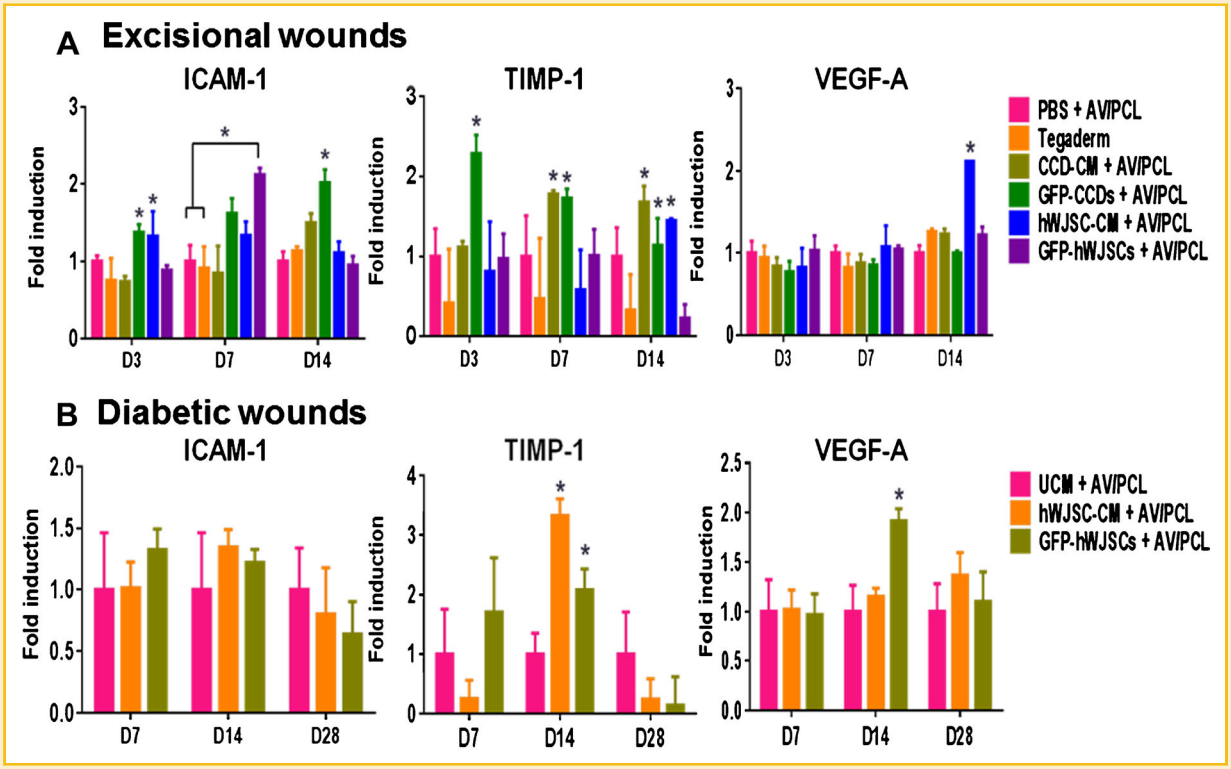

Fig. 6. (A) On day 7, ICAM-1 mRNA levels in excisional wounds of mice treated with GFP-hWJSCs + AV/PCL were significantly higher than controls while TIMP-1 and VEGF-A expression for the hWJSC-CM + AV/PCL treatment arm was significantly higher than all other groups on day 14 ($P < 0.05$). (B) For diabetic wounds, the TIMP-1 levels for both the treatment groups (GFP-hWJSCs + AV/PCL and hWJSC-CM + AV/PCL) were significantly higher on day 14 compared to other groups while VEGF-A expression was significantly higher only for the GFP-hWJSCs + AV/PCL treatment group compared to other groups on day 14 ($P < 0.05$).

of cytokines of the interleukin family [Fong et al., 2011]. The ECM is comprised of fibronectin that provides fibroblast migration and collagen and elastin that provide tissue strength and resiliency. These three proteins were produced in high concentrations in the present study which suggests their contribution to the wound healing process.

Although the use of hWJSCs or hWJSC-CM alone may enhance wound healing without the need for a nanoscaffold, the major drawback would be the short half-life of their secreted proteins due to inactivation by protease inhibitors that enrich the wound site [Murphy and Nagase, 2008]. The development of nanoscale systems for drug delivery enhances the biological efficacy of molecules via controlled release for long periods of time [Maham et al., 2009]. To overcome the inadequate expression of angiogenic factors and low cell viability after transplantation, nanotechnology has provided non-microbial, biodegradable polymeric nanoparticles to deliver the hVEGF gene to human MSC and embryonic stem cell (ESC)-derived cells [Yang et al., 2010]. Four weeks after intramuscular injection into mouse ischemic hind limbs, such genetically modified stem cells enhanced angiogenesis and salvation of limbs while reducing muscle degeneration and tissue fibrosis [Yang et al., 2010]. These findings suggest the important role of the nanoscaffold and that stem cells incorporated into such biodegradable nanoscaffolds may be of tremendous therapeutic value for vascularizing tissue constructs and treating ischemic diabetic wounds. We conclude that hWJSCs may be a better substitute to hBMMSCs for wound healing given its several advantages and together with the synergistic benefits of a nanoscaffold they make ideal combinations as wound dressings for slow healing and hard-to-heal chronic wounds.

REFERENCES

Badiavas EV, Falanga V. 2003. Treatment of chronic wounds with bone marrow-derived cells. Arch Dermatol 139:510–516.

Bao P, Kodra A, Tomic-Canic M, Golinko MS, Ehrlich HP, Brem H. 2009. The role of vascular endothelial growth factor in wound healing. J Surg Res 153:347–358.

Bongso A, Fong CY. 2013. The therapeutic potential, challenges and future clinical directions of stem cells from the Wharton's jelly of the human umbilical cord. Stem Cell Rev 9:226–240.

Brower J, Blumberg S, Carroll E, Pastar I, Brem H, Chen W. 2011. Mesenchymal stem cell therapy and delivery systems in nonhealing wounds. Adv Skin Wound Care 24:524–532.

Chen L, Tredget EE, Liu C, Wu Y. 2009. Analysis of allogenicity of mesenchymal stem cells in engraftment and wound healing in mice. PLoS ONE 4:e7119.

Chithra P, Sajithlal GB, Chandrakasan G. 1998. Influence of Aloe vera on collagen characteristics in healing dermal wounds in rats. Mol Cell Biochem 181:71–76.

Cory G. 2011. Scratch-wound assay. Methods Mol Biol 769:25–30.

Fong CY, Chak LL, Biswas A, Tan JH, Gauthaman K, Chan WK, Bongso A. 2011. Human Wharton′s jelly stem cells have unique transcriptome profiles compared to human embryonic stem cells and other mesenchymal stem cells. Stem Cell Rev 7:1–16.

Fong CY, Richards M, Manasi N, Biswas A, Bongso A. 2007. Comparative growth behaviour and characterization of stem cells from human Wharton′s jelly. Reprod Biomed Online 15:708–718.

Fong CY, Subramanian A, Biswas A, Gauthaman K, Srikanth P, Hande MP, Bongso A. 2010. Derivation efficiency, cell proliferation, freeze-thaw survival, stem-cell properties and differentiation of human Wharton′s jelly stem cells. Reprod Biomed Online 21:391–401.

Fong CY, Tam K, Cheyyatraivendran S, Gan SU, Gauthaman K, Armugam A, Jeyaseelan K, Choolani M, Biswas A, Bongso A. 2013. Human umbilical cord Wharton′s jelly stem cells and its conditioned medium enhance healing of excisional and diabetic wounds. J Cell Biochem doi: 10.1002/jcb.24661

Hamman JH. 2008. Composition and applications of Aloe vera leaf gel. Molecules 13:1599–1616.

Jackson WM, Nesti LJ, Tuan RS. 2012. Concise review: Clinical translation of wound healing therapies based on mesenchymal stem cells. Stem Cells Transl Med 1:44–50.

Jeon YK, Jang YH, Yoo DR, Kim SN, Lee SK, Nam MJ. 2010. Mesenchymal stem cells′ interaction with skin: Wound-healing effect on fibroblast cells and skin tissue. Wound Repair Regen 18:655–661.

Ji R, Cheng Y, Yue J, Yang J, Liu X, Chen H, Dean DB, Zhang C. 2007. MicroRNA expression signature and antisense-mediated depletion reveal an essential role of MicroRNA in vascular neointimal lesion formation. Circ Res 100:1579–1588.

Kawachi Y, Fujisawa Y, Furuta J, Nakamura Y, Ishii Y, Otsuka F. 2011. Superficial epithelioma with sebaceous differentiation: Immunohistochemical study of keratinocyte differentiation markers. Eur J Dermatol 21:1016–1017.

Kuzuya H, Tamai I, Beppu H, Shimpo K, Chihara T. 2001. Determination of aloenin, barbaloin and isobarbaloin in aloe species by micellar electrokinetic chromatography. J Chromatogr B Biomed Sci Appl 752:91–97.

Liao B, Bao X, Liu L, Feng S, Zovoilis A, Liu W, Xue Y, Cai J, Guo X, Qin B, Zhang R, Wu J, Lai L, Teng M, Niu L, Zhang B, Esteban MA, Pei D. 2011. MicroRNA cluster 302–367 enhances somatic cell reprogramming by accelerating a mesenchymal-to-epithelial transition. J Biol Chem 286: 17359–17364.

Liu Y, Min D, Bolton T, Nube V, Twigg SM, Yue DK, McLennan SV. 2009. Increased matrix metalloproteinase-9 predicts poor wound healing in diabetic foot ulcers. Diabetes Care 32:117–119.

Luo G, Cheng W, He W, Wang X, Tan J, Fitzgerald M, Li X, Wu J. 2010. Promotion of cutaneous wound healing by local application of mesenchymal stem cells derived from human umbilical cord blood. Wound Repair Regen 18:506–513.

Ma K, Liao S, He L, Lu J, Ramakrishna S, Chan CK. 2011. Effects of nanofiber/stem cell composite on wound healing in acute full-thickness skin wounds. Tissue Eng Part A 17:1413–1424.

Madhyastha R, Madhyastha H, Nakajima Y, Omura S, Maruyama M. 2012. MicroRNA signature in diabetic wound healing: Promotive role of miR-21 in fibroblast migration. Int Wound J 9:355–361.

Maham A, Tang Z, Wu H, Wang J, Lin Y. 2009. Protein-based nanomedicine platforms for drug delivery. Small 5:1706–1721.

Maxson S, Lopez EA, Yoo D, Danilkovitch-Miagkova A, Leroux MA. 2012. Concise review: Role of mesenchymal stem cells in wound repair. Stem Cells Transl Med 1:142–149.

Mendonca FA, Passarini JR Junior, Esquisatto MA, Mendonca JS, Franchini CC, Santos GM. 2009. Effects of the application of Aloe vera (L.) and microcurrent on the healing of wounds surgically induced in Wistar rats. Acta Cir Bras 24:150–155.

Murphy G, Nagase H. 2008. Progress in matrix metalloproteinase research. Mol Aspects Med 29:290–308.

Ndhlala AR, Amoo SO, Stafford GI, Finnie JF, Van Staden J. 2009. Antimicrobial, anti-inflammatory and mutagenic investigation of the South African tree aloe (Aloe barberae). J Ethnopharmacol 124:404–408.

Shaw TJ, Martin P. 2009. Wound repair at a glance. J Cell Sci 122:3209–3213.

Shilo S, Roth S, Amzel T, Harel-Adar T, Tamir E, Grynspan F, Shoseyov O. 2013. Cutaneous wound healing after treatment with plant-derived human recombinant collagen flowable gel. Tissue Eng Part A 19:1519–1526.

Shin L, Peterson DA. 2013. Human mesenchymal stem cell grafts enhance normal and impaired wound healing by recruiting existing endogenous tissue stem/progenitor cells. Stem Cells Transl Med 2:33–42.

Stevens LJ, Page-McCaw A. 2012. A secreted MMP is required for reepithelialization during wound healing. Mol Biol Cell 23:1068–1079.

Sullivan SR, Underwood RA, Gibran NS, Sigle RO, Usui ML, Carter WG, Olerud JE. 2004. Validation of a model for the study of multiple wounds in the diabetic mouse (db/db). Plast Reconstr Surg 113:953–960.

Takzare N, Hosseini MJ, Hasanzadeh G, Mortazavi H, Takzare A, Habibi P. 2009. Influence of Aloe Vera gel on dermal wound healing process in rat. Toxicol Mech Methods 19:73–77.

Tocco I, Zavan B, Bassetto F, Vindigni V. 2012. Nanotechnology-based therapies for skin wound regeneration. J Nanomater Article ID 714134. doi: 10.1155/2012/714134

Vazquez B, Avila G, Segura D, Escalante B. 1996. Antiinflammatory activity of extracts from Aloe vera gel. J Ethnopharmacol 55:69–75.

Walter MN, Wright KT, Fuller HR, MacNeil S, Johnson WE. 2010. Mesenchymal stem cell-conditioned medium accelerates skin wound healing: An in vitro study of fibroblast and keratinocyte scratch assays. Exp Cell Res 316:1271–1281.

White-Chu EF, Flock P, Struck B, Aronson L. 2011. Pressure ulcers in long-term care. Clin Geriatr Med 27:241–258.

Wu Y, Chen L, Scott PG, Tredget EE. 2007. Mesenchymal stem cells enhance wound healing through differentiation and angiogenesis. Stem Cells 25:2648–2659.

Yang F, Cho SW, Son SM, Bogatyrev SR, Singh D, Green JJ, Mei Y, Park S, Bhang SH, Kim BS, Langer R, Anderson DG. 2010. Genetic engineering of human stem cells for enhanced angiogenesis using biodegradable polymeric nanoparticles. Proc Natl Acad Sci USA 107:3317–3322.